ACS OMEGA

http://pubs.acs.org/journal/acsodf

Article

Photoelectrochemical Oxidation of Amines to Imines and Production of Hydrogen through Mo-Doped $BiVO_4$ Photoanode

Yujie He, Haipeng Zhang, Zeyan Wang,* Zhaoke Zheng, Peng Wang, Yuanyuan Liu, Hefeng Cheng, Xiaoyang Zhang, Ying Da, and Baibiao Huang*

Cite This: *ACS Omega* 2022, 7, 12816−12824

Read Online

ACCESS | Metrics & More | Article Recommendations | Supporting Information

ABSTRACT: Imines are important multifunctional intermediates for the synthesis of pesticides, pharmaceuticals, biologics, and fine chemicals. The direct photoelectrochemical (PEC) oxidation of amines to imines is a highly selective, efficient, green, and gentle method. Interestingly, the constructive merging of the PEC oxidation of amines with the production of hydrogen can accelerate hydrogen evolution due to the less challenging oxidation of amines such as benzylamine (BN) in comparison to sluggish water oxidation. Herein, Mo-doped $BiVO_4$ photoanodes were prepared and first applied to simultaneously oxide benzylamine (BN) to *N*-benzylidenebenzylamine (BI) and produce hydrogen in a closed two-chamber, three-electrode PEC cell After illumination at a bias of 1.3 V vs SCE for 3 h, the 3% Mo-doped $BiVO_4$ photoanode achieved a maximum yield of ∼94 μmol h^{-1} at a 1 × 1 cm^2 area with a BN to BI selectivity of almost 100% and a Faradaic efficiency of 98.4%. Our electrode presented enhanced photocorrosion resistance in acetonitrile solvent. Additionally, the PEC oxidations of benzylamine derivatives with different substituents (−F, −Cl, −Br, $-CH_3$, $-OCH_3$) to the corresponding imines were also investigated. The results indicated that the Mo-doped $BiVO_4$ photoanode exhibited an excellent performance in the oxidation of these benzylamine derivatives with corresponding amine to imine selectivities of almost 100% and Faradaic efficiencies of >95%.

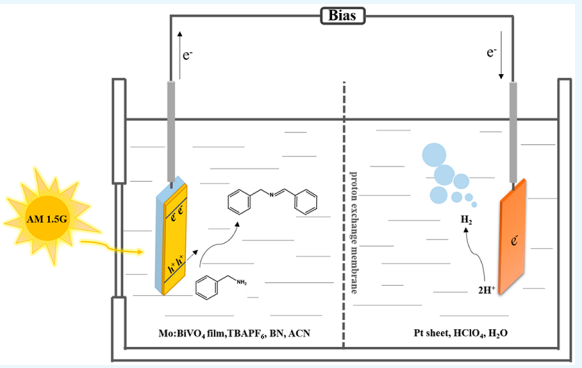

1. INTRODUCTION

The selective oxidation of amines to the corresponding imines is an important transformation reaction in organic chemistry due to the wide applications of the product imines and their derivatives in the fields of pharmaceuticals, pesticides, biologics, and fine chemicals.[1−6] Traditionally, imines are produced by the condensation of primary amines with carbonyl compounds.[7−10] However, toxic oxidants, expensive dehydrating agents, high temperature, and unstable aldehydes or ketones are usually involved in these processes, which are environmentally hazardous, uneconomical, uncontrollable, and inefficient. Thus, the exploration of new strategies that can directly oxidize amines to imines in a more controllable, efficient, and eco-friendly manner is highly desired.[11−13]

From the perspective of green chemistry, the direct photocatalytic or electrocatalytic oxidation of amines is a more attractive method. However, both methods suffer from defects. On the basis of sunlight and molecular oxygen, the direct photocatalytic oxidation of amines is green, mild, and economical. Despite the high product selectivity (>90%) achieved, the poor activity remains a headache. Long hours of illumination are usually indispensable for an ideal conversion rate and yield.[14−17] Different from photocatalysis, electrocatalysis can actively oxide amines with an external energy input. Unfortunately, nitriles tend to be formed due to the peroxidation of unstable imine intermediates, resulting in a poor product selectivity.[18−20]

As the merging of photocatalysis and electrocatalysis, a photoelectrochemical (PEC) catalysis is expected to combine the advantages of both methods, which has been proven to be an effective method for the oxidation of some organic substrates with high conversion efficiencies and selectivities.[21] Additionally, the substitution of the sluggish water oxidation with the less challenging oxidation of organic substrates could subsequently promote hydrogen evolution at the counter electrode.[22−25] For instance, researchers have carried out the TEMPO-mediated PEC oxidation of 5-hydroxymethylfurfural (HMF) to 2,5-furandicarboxylic acid (FDCA),[26−28] the PEC coupling of 5-amino-1*H*-tetrazole (5AT) to 5,5′-azotetrazolate (SZT),[29,30] and the PEC selective oxidation of glycerol to 1,3-dihydroxyacetone (DHA).[31−33] Thus, a PEC process is also

Received: January 4, 2022
Accepted: March 24, 2022
Published: April 7, 2022

https://doi.org/10.1021/acsomega.2c00048
ACS Omega 2022, 7, 12816−12824

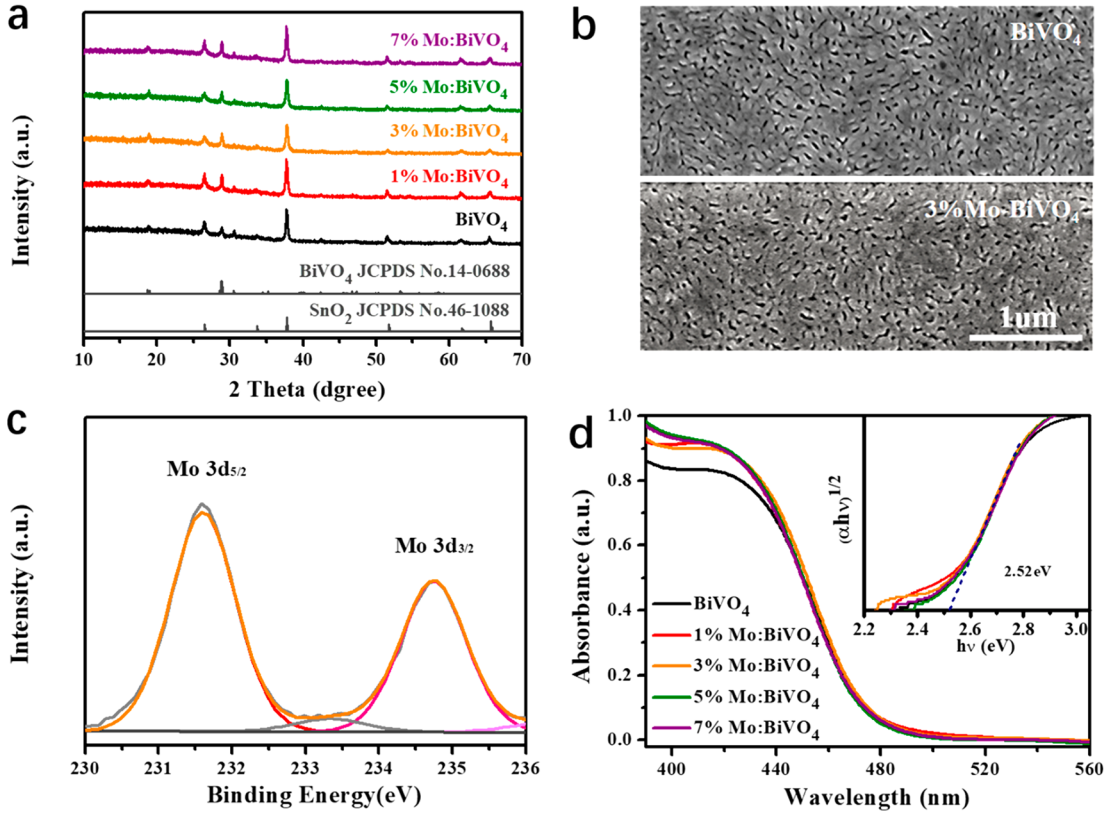

Figure 1. (a) XRD patterns and (b) SEM images of as-prepared pristine $BiVO_4$ and *X*% Mo:$BiVO_4$ (*X* = 1, 3, 5, 7) electrodes. (c) Mo 3d XPS elemental spectrum of the 3% Mo:$BiVO_4$ electrode. (d) Diffuse reflectance absorption spectrum of pristine $BiVO_4$ and *X*% Mo:$BiVO_4$ (*X* = 1, 3, 5, 7) electrodes. The inset gives the Tauc plots of all electrodes.

expected to be able to convert amines to imines with high conversion efficiency and selectivity. Moreover, the constructive merging of the less challenging oxidation of amines on a photoanode with the production of hydrogen on a photocathode in one PECcell is beneficial, which can not only produce high-value-added imines but also achieve the high-rate production of hydrogen—an emerging energy with great application potential in the future.[34−37]

To address the above assumption, Mo-doped $BiVO_4$, as one of the most promising materials with an appropriate band gap and high theoretical photocurrent,[38−40] was selected as the photoanode. The direct oxidation of benzylamine (BN) to *N*-benzylidenebenzylamine (BI) was chosen as the model reaction. The experimental results indicated that the selective oxidation of BN to BI with high efficiency along with high-rate hydrogen evolution could be achieved over a Mo-doped $BiVO_4$ photoanode under the continuous irradiation of simulated solar light. Additionally, the use of the PEC oxidation of benzylamine derivatives containing different substituents, i.e., −F, −Cl, −Br, $-CH_3$, and $-OCH_3$, was also investigated, in which benzylamine derivatives could be oxidized into the corresponding imines over a 3% Mo-doped $BiVO_4$ photoanode. Our results indicate that PEC organic synthesis may offer an ideal method for the selective oxidation of amines to imines on a large scale in the future.

2. RESULTS AND DISCUSSION

Pristine $BiVO_4$ and Mo-doped $BiVO_4$ electrodes were fabricated by spin coating followed by a subsequent annealing treatment (Figure S1). The concentrations of Mo, defined as atomic percent, were respectively 1%, 3%, 5%, and 7% with respect to V content. The structures and morphologies of the as-prepared electrodes were characterized by X-ray diffraction (XRD), X-ray photoelectron spectroscopy (XPS), and scanning electron microscopy (SEM). As shown in Figure 1a, all of the XRD patterns of the prepared $BiVO_4$ or Mo-doped $BiVO_4$ electrodes can be indexed to monoclinic $BiVO_4$ (JCPDS No. 14-0688) in addition to some diffraction peaks corresponding to the FTO (F:SnO_2) substrate (JCPDS No. 46-1088). The similar XRD patterns of all electrodes indicates that the addition of trace Mo has little effect on the crystalline structure. SEM images (Figure 1b) show that both the pristine $BiVO_4$ and 3% Mo-doped $BiVO_4$ electrodes are composed of irregular nanoparticles with a diameter of 150−200 nm, which indicates that the morphology of $BiVO_4$ was not changed by the doping of trace Mo. The mapping images of SEM (Figure S2) shows that the four elements Bi, V, Mo, and O are evenly distributed in the 3% Mo-doped $BiVO_4$ electrode, which proves the successful doping of Mo. High-resolution elemental scans for the 3% Mo-doped $BiVO_4$ electrode were executed by XPS. Two characteristic peaks corresponding to the $3d_{3/2}$ and $3d_{5/2}$ orbitals of Mo^{6+}, respectively, can be observed, which proves the existence of Mo in a hexavalent state (Figure 1c). The diffuse reflectance absorption spectrum of as-prepared electrodes was measured with a UV−vis spectrophotometer. All electrodes exhibit almost identical absorption curves with absorption edges at around 480 nm, and the band gaps are estimated to be approximately 2.52 eV (Figure 1d), which indicates that the doping of Mo^{6+} did not change the band gap and light absorption properties of the materials.

https://doi.org/10.1021/acsomega.2c00048
ACS Omega 2022, 7, 12816−12824

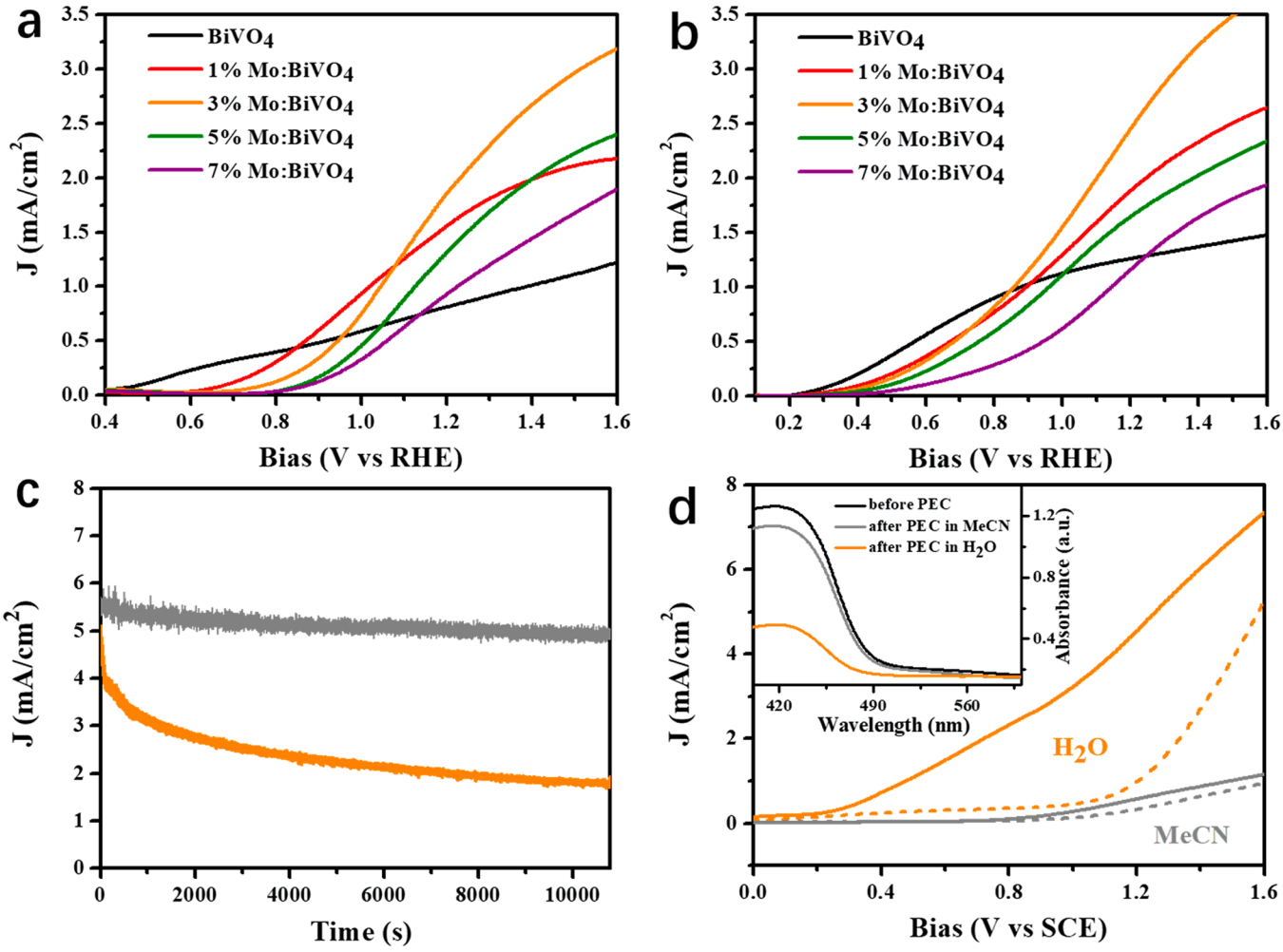

Figure 2. $J-V$ plots of the as-prepared pristine $BiVO_4$ and X% Mo:$BiVO_4$ (X = 1, 3, 5, 7) electrodes measured in a 0.1 M potassium phosphate electrolyte (a) without and (b) with 0.05 M BN upon illumination with an AM 1.5G filtered solar simulator. (c) $I-t$ curves of the 3% Mo:$BiVO_4$ electrode measured at a constant bias of 1.3 V vs SCE in a 0.1 M potassium phosphate electrolyte with 0.05 M BN (orange) and in a 0.1 M $TBAPF_6$ acetonitrile solution with 0.05 M BN (gray) under continued light irradiation. (d) $J-V$ plots of the 3% Mo:$BiVO_4$ electrode before (solid line) and after (dashed line) PEC electrolysis for 36 h in water (orange) or acetonitrile (gray). The inset shows the absorption spectra of the 3% Mo:$BiVO_4$ electrode before (black) and after PEC electrolysis for 36 h in water (orange) or acetonitrile (gray).

The difficulties of the benzylamine oxidation reaction (BOR) and oxygen evolution reaction (OER) were first compared with a three-electrode PEC cell with the as-prepared $BiVO_4$ and X% Mo:$BiVO_4$ (X = 1, 3, 5, 7) electrodes as working electrodes, a platinum sheet (Pt) as the counter electrode, and a saturated calomel electrode (SCE) as the reference electrode. We explored the OER performances of our electrodes in a 0.1 M potassium phosphate aqueous solution. The $J-V$ curves (Figure 2a) show a significant increase of the photocurrent density in Mo-doped $BiVO_4$ electrodes with a slightly higher onset potential of ~0.7 V vs RHE with respect to the pristine $BiVO_4$ electrode. Among them, the 3% Mo-doped $BiVO_4$ electrode obtains the optimum photocurrent density of up to 1.98 mA/cm^2 at a bias of 1.23 V vs RHE, while the pristine $BiVO_4$ electrode merely has a 0.84 mA/cm^2 density at the same bias. However, when the doping concentration of Mo^{6+} continues to increase, the photocurrent density decreases. Then, we explored the BOR performances of our electrodes in a 0.1 M potassium phosphate aqueous solution containing 0.05 M BN. As shown in the $J-V$ curves (Figure 2b), our electrodes have an onset potential of ~0.4 V vs RHE and achieve an obviously negative shift of ~300 mV relative to that of the OER. The change in the $J-V$ curves is consistent with the above test results, but the photocurrents of all electrodes increase to some extent in comparison with the OER. This experimental phenomenon preliminarily proves that the BOR is less challenging to carry out on the $BiVO_4$ electrodes in comparison to the sluggish water oxidation. The PEC stability of the 3% Mo-doped $BiVO_4$ electrode was tested at a constant bias of 1.3 V vs SCE in a 0.1 M potassium phosphate aqueous solution containing 0.05 M BN under simulated AM1.5G sunlight irradiation for 3 h. Unfortunately, an obvious attenuation of photocurrent density along with time can be observed from the $I-t$ curves (Figure 2c, orange), which results from the high-rate photocorrosion of $BiVO_4$ electrodes in the aqueous phase. Acetonitrile has recently emerged as a promising solvent in organic systhesis due to its two key properties: (a) an excellent ability to dissolve considerable polar and nonpolar solutes and (b) relative inertia to avoid unfavorable side reactions.[41−44] As shown in Figure S3, BN exhibits superior solubility in acetonitrile in comparison to that in water. Moreover, the photocurrent

https://doi.org/10.1021/acsomega.2c00048
ACS Omega 2022, 7, 12816−12824

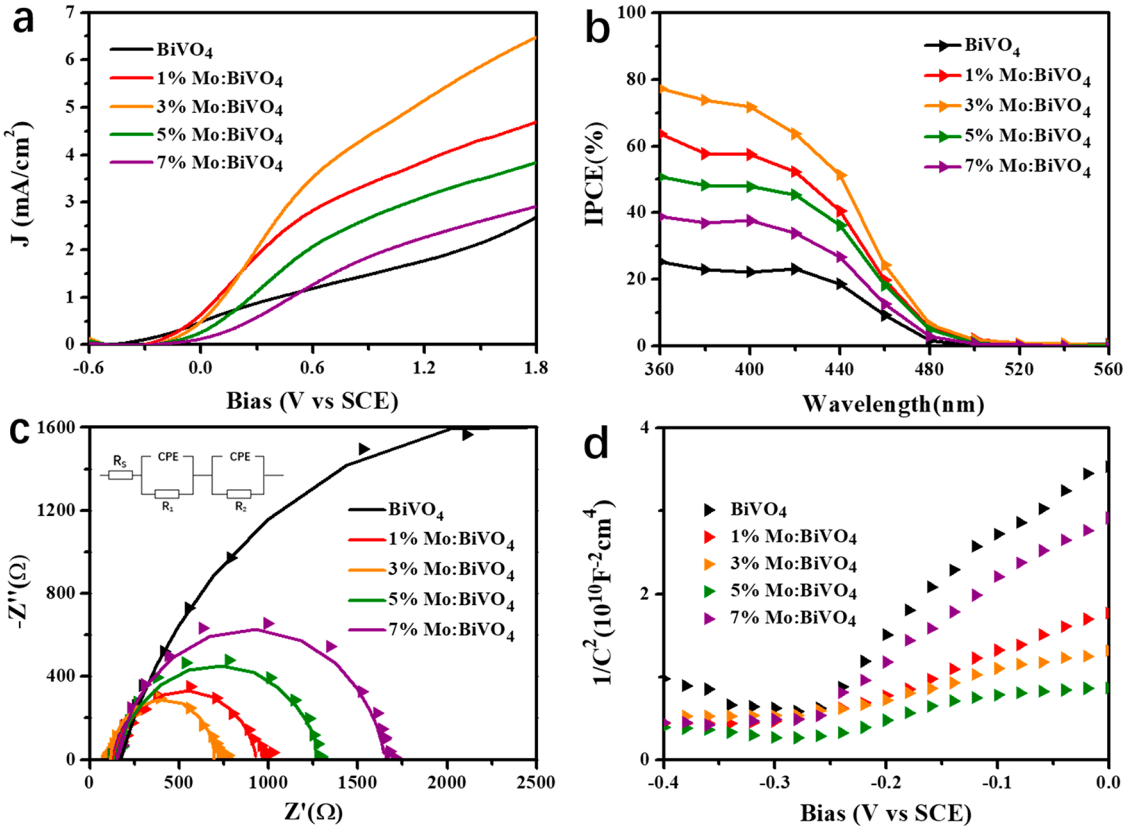

Figure 3. (a) $J-V$ plots of the as-prepared electrodes measured at a scan rate of 20 mV/s upon illumination with an AM 1.5G filtered solar simulator. (b) Monochromatic incident photon to electron conversion efficiencies (IPCEs) of the as-prepared electrodes measured at a bias of 1.3 V vs SCE. (c) Nyquist plots of the as-prepared electrodes measured at a bias of 1.3 V vs SCE upon light illumination. (d) Mott−Schottky plots of the as-prepared electrodes measured at a frequency of 1 kHz in the dark. All of the tests were performed in a 0.1 M $TBAPF_6$ acetonitrile solution containing 0.05 M BN.

density of the 3% Mo-doped $BiVO_4$ electrode in 0.1 M tetrabutylammonium hexafluorophosphate ($TBAPF_6$) acetonitrile solution without the addition of BN is very low (Figure S4), which indicates that the competitive effect of acetonitrile as solvent on the BOR can be ignored. Thus, using acetonitrile as an alternative solvent is an attractive strategy. Furthermore, the photocorrosion rates of 3% Mo-doped $BiVO_4$ electrodes in water and acetonitrile were investigated. The 3% Mo-doped $BiVO_4$ electrodes were immersed in a 0.1 M potassium phosphate aqueous solution or a 0.1 M $TBAPF_6$ acetonitrile solution and exposed to irradiation for 36 h at biases of 0.5 and 1.3 V vs SCE, respectively. The $J-V$ curves (Figure 2d) show that the photocurrent density of the electrode after PEC electrolysis in water is severely attenuated while that of the electrode after PEC electrolysis in acetonitrile decays only slightly. The absorption spectra of 3% Mo-doped $BiVO_4$ electrodes after PEC electrolysis were also measured. As shown in the inset of Figure 2d, a more significant attenuation in intensity over the range of 400−500 nm in water in comparison to that in acetonitrile can be observed. The PEC stability of the 3% Mo-doped $BiVO_4$ electrode was further measured at a constant bias of 1.3 V vs SCE in 0.1 M $TBAPF_6$ acetonitrile solution containing 0.05 M BN under simulated AM1.5G sunlight irradiation for 3 h. Only a slight attenuation of photocurrent density along with time was observed from the $I-t$ curve (Figure 2c, gray). The experimental results prove that the high-rate photocorrosion of the $BiVO_4$ electrode in water can be effectively suppressed by the use of acetonitrile as the solvent. In addition, acetonitrile as an alternative solvent results in an enlarged range of organic substrates due to its excellent solvation properties.

The BOR performances of the electrodes were further investigated in a 0.1 M $TBAPF_6$ acetonitrile solution containing 0.05 M BN. The change in photocurrent density obtained from the $J-V$ plots (Figure 3a) is in accord with that of the photocurrent density measured previously in the aqueous phase electrolyte. Likewise, the 3% Mo-doped $BiVO_4$ electrode achieves the highest photocurrent density of about 5.39 mA/cm^2 at 1.3 V vs SCE, which is about 3 times higher than the photocurrent density of the pristine $BiVO_4$ electrode. When the doping concentration of Mo^{6+} is increased to 5% or 7%, the values of the photocurrent density decrease. The monochromatic incident photon to electron conversion efficiencies (IPCEs) of pristine $BiVO_4$ and Mo-doped $BiVO_4$ electrodes were measured. The IPCE values of $BiVO_4$ electrodes are increased by Mo^{6+} doping, and the 3% Mo-doped $BiVO_4$ electrode achieves an optimal value about 64% while that of the pristine $BiVO_4$ electrode is only 23% at a wavelength of 420 nm (Figure 3b). When the doping concentration of Mo^{6+} is increased to 5% or 7%, the values of IPCEs also decrease. As we all know, the IPCE value is relevant to the absorptivity and carrier separation properties of the electrodes. We have demonstrated that doping did not change the absorptivity of the electrodes; thus, the change in IPCE values is related to the carrier separation and electrical properties of the electrodes. Electrochemical impendence

https://doi.org/10.1021/acsomega.2c00048
ACS Omega 2022, 7, 12816−12824

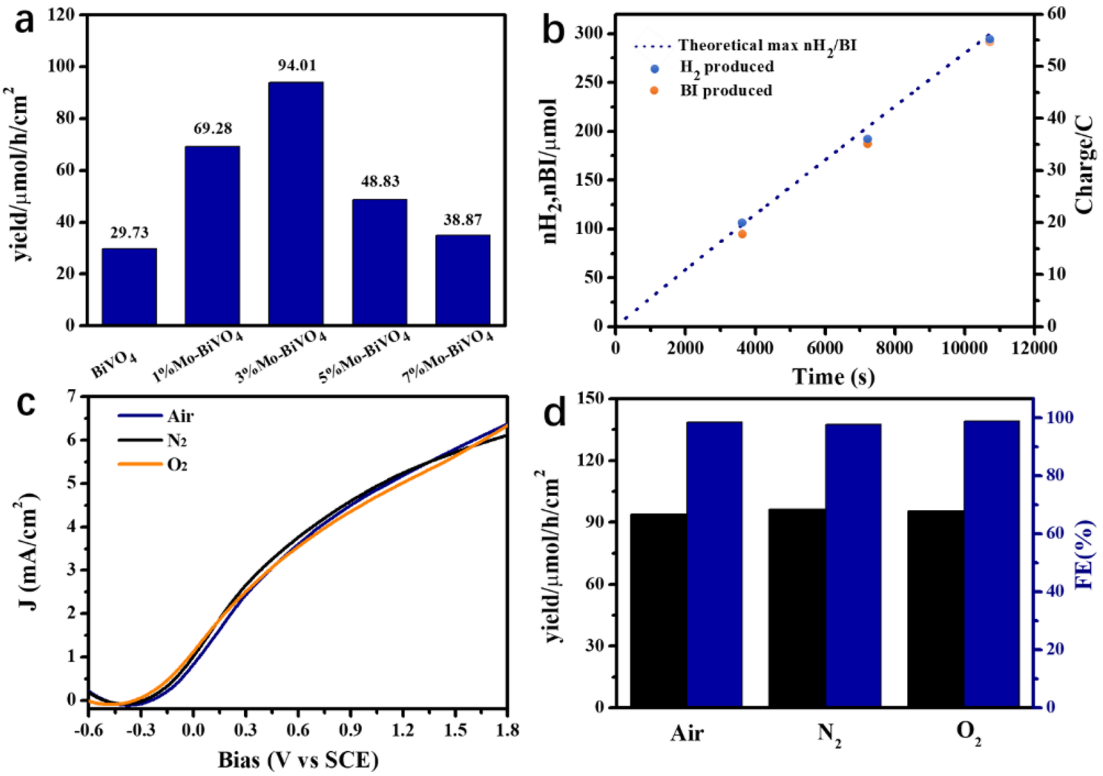

Figure 4. (a) Yields of BI obtained by the pristine $BiVO_4$ and *X*% Mo:$BiVO_4$ (*X* = 1, 3, 5, 7) electrodes after an AM 1.5G filtered solar simulator illumination for 3 h. (b) Actual yields and theoretical yields of H_2 and BI derived from a chronoamperometric experiment at a bias of 1.3 V vs SCE by the 3% Mo:$BiVO_4$ electrode under an AM 1.5G filtered solar simulator illumination for 3 h. (c) *J*−*V* plots of the 3% Mo:$BiVO_4$ electrodes measured under different atmospheres. (d) Yields of BI and the Faradaic efficiencies of the coupling reaction obtained by the 3% Mo:$BiVO_4$ electrodes under different atmospheres.

Table 1. Oxidative Coupling of Various Amines to Corresponding Imines through a 3% Mo:$BiVO_4$ Electrode

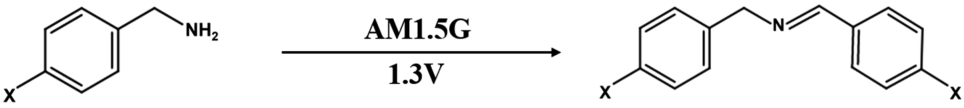

entry	substrate	product	*t* (h)	Q (C)	n_{e-} (μmol)	yield (μmol)	FE (%)	SEL (%)
1	X = H	X = H	3	55.23	573.22	282.03	98.40	>99
2	X = p-F	X = p-F	3	54.83	569.13	279.21	98.12	>99
3	X = p-Cl	X = p-Cl	3	56.19	583.20	283.52	97.23	>99
4	X = p-Br	X = p-Br	3	55.99	581.16	282.85	97.34	>99
5	X = p-CH_3	X = p-CH_3	3	53.69	557.27	273.23	98.06	>99
6	X = p-OCH_3	X = p-OCH_3	3	49.58	514.59	247.47	96.18	>99

spectra analyses and Mott−Schottky measurements were carried out to investigate the charge separation and electrical conductivity properties of the as-prepared electrodes. The charge transfer resistances of the pristine $BiVO_4$ and *X*% Mo:$BiVO_4$ (*X* = 1, 3, 5, 7) electrodes obtained from an equivalent circuit by fitting the Nyquist plots (Figure 3c) are estimated to be 4.4, 0.8, 0.6, 1.2, and 1.5 kΩ, respectively, which illustrates that the electrical conductivity of the pristine $BiVO_4$ electrode can be promoted by Mo^{6+} doping and the change trend is consistent with the photocurrent density. The carrier concentration of pristine $BiVO_4$ and *X*% Mo:$BiVO_4$ (*X* = 1, 3, 5, 7) electrodes extracted from the Mott−Schottky plots (Figure 3d) are calculated to be 1.41×10^{19}, 5.29×10^{19}, 6.12×10^{19}, 5.01×10^{19}, and 1.96×10^{19} cm^{-3}, respectively, which demonstrates that the donor density can be improved by Mo^{6+} doping and the change trend is also similar to those of the photocurrent densities and resistances. These experimental results show that the doping of trace Mo^{6+} can promote electron−hole separation and increase carrier density and electrical conductivity, which can improve the PEC performances of our electrodes. However, when the Mo^{6+} doping amount is large enough, it can serve as a new electron−hole composite center and reduce the length of electron diffusion, which further limits the improvement in the PEC performances of our electrodes. This is in accord with previous reports.[45−47]

The dark current of the $BiVO_4$ electrode for BOR were measured in 0.1 M $TBAPF_6$ acetonitrile solution containing 0.05 M BN. The *J*−*V* plots (Figure S5a) show that the electrochemical BOR occurs slightly after a bias of ∼1.5 V vs SCE. Thus, 1.3 V vs SCE was selected as the reaction bias to avoid the electrochemical BOR and give a considerable yield. Additionally, the yield and selectivity of oxidation of BN to BI by only photocatalysis or electrocatalysis were also inves-

https://doi.org/10.1021/acsomega.2c00048
ACS Omega 2022, 7, 12816−12824

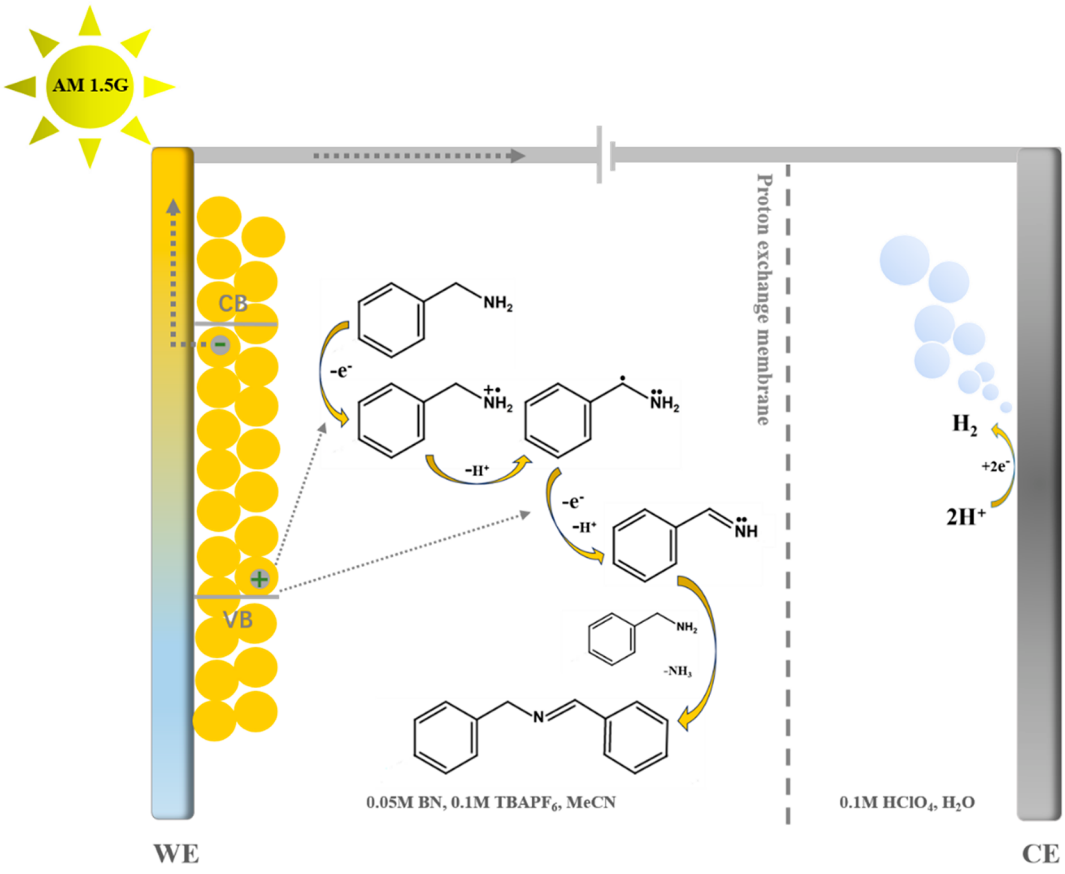

Figure 5. Proposed mechanism of PEC coupling of amines to imines over a Mo:$BiVO_4$ electrode.

tigated. As shown in Figure S5b, the PEC oxidation of BN to BI can result in a high yield and selectivity, which could not be achieved by single electrocatalysis or photocatalysis, and the PEC oxidation of BN to BI at 1.3 V vs SCE is the result of the synergistic effect of photocatalysis and electrocatalysis. A chronoamperometry experiment was implemented in a closed two-chamber, three-electrode PEC cell with proton transfer between the two chambers via a proton exchange membrane. Efficient H_2 evolution can be observed during the reaction process (Figure S6). After a PEC reaction for 3 h, the anode products were detected by a gas chromatograph equipped with a flame ionization detector. The BI yields of pristine $BiVO_4$ and *X*% Mo:$BiVO_4$ (*X* = 1, 3, 5, 7) electrodes are 29.73, 69.28, 94.01, 48.83, 38.87 μmol/(h cm^2), respectively (Figure 4a). The 3% Mo-doped $BiVO_4$ electrode had the best PEC performance and the maximum yield of BI. The Faradaic efficiency and selectivity of BN to BI reaction by the 3% Mo-doped $BiVO_4$ electrode were further calculated to be 98.40% and ~100%, respectively. (Table 1, entry 1). Similarly, the Faradaic efficiency for photocathode hydrogen production was also calculated to be >95%. As shown in Figure 4b, the ratio of BI yield to H_2 yield is about 1:1, and the yield is almost equal to the theoretical value.

There are usually two mechanisms of BN photooxidation. One is an aerobic mechanism, where oxygen is reduced to a superoxide radical by photogenerated electron and then participates in the oxidation process.[48−51] The other is an anaerobic mechanism, where the whole process is led by the photogenerated holes on the valence band of photoanode without the participation of superoxide radicals.[52,53] The previous PEC coupling of BN to BI over our electrodes was performed without venting the air; thus, we could not rule out the effect of oxygen in the solution and above the liquid level. Therefore, we investigated the PEC coupling of BN to BI over 3% Mo-doped $BiVO_4$ electrodes under different atmospheres. Before all of the experiments, nitrogen or oxygen was used to vent the air, and oxygen was kept flowing over the course of the experiment to prevent oxygen shortages due to excessive consumption. As shown in Figure 4c, the *J*−*V* curves measured under different atmospheres exhibit almost the same trend. Chronoamperometry experiments were also performed in a closed two-chamber, three-electrode reactor with a proton exchange membrane at a bias of 1.3 V vs SCE under irradiation for 3 h. The yields of BI and the Faraday efficiencies of coupling BN to BI after reaction for 3 h obtained by 3% Mo-doped $BiVO_4$ electrodes under N_2 and O_2 atmospheres have very little difference from the experimental results obtained in an air atmosphere (Figure 4d). This proves that superoxide radicals were not involved in the reaction and the PEC oxidative coupling of BN to BI over Mo-doped $BiVO_4$ electrodes was carried out by an anaerobic mechanism. The detailed oxidation process is shown in Figure 5. First, BN is oxidized to generate a nitrogen-centered radical cation intermediate and the intermediate is deprotonated to form a neutral carbon radical intermediate. Then, the intermediate is oxidized and deprotonated to form an imine followed by a simple condensation reaction with another BN, producing BI. Each BN molecule is produced with the consumption of two holes, while the cathode consumes two electrons to produce one molecule of hydrogen.

In addition, the organic substrates could be extended to benzylamine derivatives containing electron-withdrawing sub-

https://doi.org/10.1021/acsomega.2c00048
ACS Omega 2022, 7, 12816−12824

stituents (−F, −Cl, −Br) or electron-donating substituents ($-CH_3$, $-OCH_3$). The 3% Mo-doped $BiVO_4$ electrode also exhibited good PEC performances with respect to these benzylamine derivatives. As shown in Figure S7a, the $J-V$ curves of the 3% Mo-doped $BiVO_4$ electrode for the oxidation of different benzylamine derivatives exhibit almost the same onset potential of ∼−0.3 V vs SCE with a photocurrent density higher than 5 mA/cm^2 at 1.3 V vs SCE. Chronoamperometry experiments were further implemented at a bias of 1.3 V vs SCE upon irradiation with simulated sunlight for 3 h. The 3% Mo-doped $BiVO_4$ electrodes show good stability in electrolytes containing various benzylamine derivatives during the PEC reaction process (Figure S7b−f). All of the benzylamine derivatives could be converted to the corresponding imines through a coupling reaction in considerable yields (>80 μmol/(h cm^2)), and the Faradaic efficiencies for the coupling of various benzylamine derivatives to the corresponding imines were all more than 95% and the selectivities were near 100% (Table 1, entries 2−6). These experimental results preliminarily prove that this PEC oxidative coupling reaction through the Mo-doped $BiVO_4$ photoanode has a certain universality.

3. CONCLUSIONS

The oxidation of BN and the production of H_2 were performed simultaneously in a closed two-chamber, three-electrode PEC cell using a series of Mo-doped $BiVO_4$ as the working electrode, a conventional Pt as the counter electrode and the SCE as the reference electrode. Doping with 1−7% Mo^{6+} significantly improved the PEC performances by increasing the carrier concentration and enhancing the conductivity, of which the 3% Mo-doped $BiVO_4$ electrode achieved the optimal PEC performance. An ∼94.01 μmol/(h cm^2) yield of BI could be achieved along with the production of homologous stoichiometric H_2 with the 3% Mo-doped $BiVO_4$ electrode. Both the oxidation of BI and the production of H_2 display more than 95% Faradaic efficiencies and nearly 100% selectivities. This coupling reaction has a certain universality, and the organic substrates can be extended to some benzylamine derivatives. This work achieves both the efficient PEC production of H_2 and high-value-added products, which indicates that PEC may offer a mild, green, and efficient pathway for the large-scale production of imines in the future.

4. EXPERIMENTAL SECTION

4.1. Photoanode Preparation. $BiVO_4$ and Mo:$BiVO_4$ electrodes were fabricated by spin coating with a subsequent annealing treatment. For the $BiVO_4$ precursor solution, 0.4 M $Bi(NO_3)_3{\cdot}5H_2O$ was dissolved in 1.8 mL of glacial acetic acid and 0.06 M vanadyl acetylacetonate was dissolved in 12 mL of acetylacetone, and the two solutions were mixed in a Bi:V molar ratio of 1:1. For the Mo:$BiVO_4$ precursor solutions, molybdenyl acetylacetonate was used as the Mo source for dissolution in the above precursor solution. The concentrations of Mo, defined as atomic percent, were respectively 1%, 3%, 5%, and 7% with respect to V content and the Bi:(V + Mo) molar ratio in the Mo:$BiVO_4$ precursor solution was kept at 1:1. The precursor solutions were obtained after stirring for 20 min and an ultrasonication treatment for 4 h at room temperature. The above precursor solutions were spin-coated on FTO substrates at 700 rpm for 10 s. The FTO substrates were then dried at 150 °C for 10 min and calcined at 470 °C for 30 min. The above procedures were repeated for four cycles.

4.2. Characterization. The structures and morphologies of the as-prepared electrodes were characterized by X-ray diffraction (Bruker D8 Advance with Cu Kα irradiation), scanning electron microscopy (Hitachi S-4800), and X-ray photoelectron spectroscopy (Thermo Fisher Scientific Escalab 250). The diffuse reflectance spectra were measured with a UV−vis spectrophotometer equipped with an integrating sphere (Shimadzu UV 2550).

4.3. Photoelectrochemical Measurement. The PEC measurements were performed in a three-electrode PEC cell with the as-prepared electrode as the working electrode, Pt as the counter electrode, and the SCE as the reference electrode with a Princeton Applied Research EG&G 263A potentiostat. Experiments were conducted under AM1.5G simulated sunlight with a 300 W xenon arc lamp (Perfectlight, Beijing, Co. Ltd.) coupled with an AM1.5G global filter. The anode electrolyte was a 0.1 M potassium phosphate aqueous solution or a 0.1 M $TBAPF_6$ acetonitrile solution containing 0.05 M of the organic substrates; the cathode electrolyte was a 0.1 M $HClO_4$ aqueous solution. The PEC oxidation of organic substrates and the production of H_2 were performed in a closed two-chamber, three-electrode PEC cell with a constant bias of 1.3 V vs SCE. Experimental details are provided in the Supporting Information.

■ ASSOCIATED CONTENT

Supporting Information

The Supporting Information is available free of charge at https://pubs.acs.org/doi/10.1021/acsomega.2c00048.

Detail photoelectrochemical characterization and chronoamperometry experiment; schematic diagram of the fabrication procedure of photoanodes; mapping images of the 3% Mo:$BiVO_4$ electrode; pictures of the 0.1 M BN aqueous solution and the 0.1 M BN acetonitrile solution; $J-V$ plots of the as-prepared electrodes measured in a 0.1 M $TBAPF_6$ acetonitrile solution; $I-t$ curves of $BiVO_4$ electrode measured at 1.3 V vs SCE with AM1.5G simulated sunlight and measured at 2.2 V vs SCE in dark; $J-V$ plots of $BiVO_4$ electrode measured in the 0.1 M $TBAPF_6$ acetonitrile solution; yields and selectivities of oxidation of BN to BI under different conditions; pictures of the closed two-chamber, three-electrode PEC reactor , the efficient H_2 evolution observed during the reaction process, and the organic solution after PEC reaction for 3 h; $J-V$ plots and $I-t$ curves of the 3% Mo:$BiVO_4$ electrode measured in the 0.1 M $TBAPF_6$ acetonitrile solution containing 0.05M 4-fluorobenzylamine, 4-chloroaniline, 4-bromoaniline, 4-methylbenzylamine, and 4-methoxybenzylamin (PDF)

■ AUTHOR INFORMATION

Corresponding Authors

Zeyan Wang − *State Key Laboratory of Crystal Materials, Shandong University, Jinan 250100, People's Republic of China;* orcid.org/0000-0002-0723-4956; Email: wangzeyan@sdu.edu.cn

Baibiao Huang − *State Key Laboratory of Crystal Materials, Shandong University, Jinan 250100, People's Republic of China;* orcid.org/0000-0002-0416-944X; Email: bbhuang@sdu.edu.cn

https://doi.org/10.1021/acsomega.2c00048
ACS Omega 2022, 7, 12816−12824

Authors

Yujie He − *State Key Laboratory of Crystal Materials, Shandong University, Jinan 250100, People's Republic of China*

Haipeng Zhang − *State Key Laboratory of Crystal Materials, Shandong University, Jinan 250100, People's Republic of China*

Zhaoke Zheng − *State Key Laboratory of Crystal Materials, Shandong University, Jinan 250100, People's Republic of China;* orcid.org/0000-0003-1104-2583

Peng Wang − *State Key Laboratory of Crystal Materials, Shandong University, Jinan 250100, People's Republic of China;* orcid.org/0000-0003-4250-8104

Yuanyuan Liu − *State Key Laboratory of Crystal Materials, Shandong University, Jinan 250100, People's Republic of China;* orcid.org/0000-0002-9453-6943

Hefeng Cheng − *State Key Laboratory of Crystal Materials, Shandong University, Jinan 250100, People's Republic of China;* orcid.org/0000-0002-9135-8109

Xiaoyang Zhang − *State Key Laboratory of Crystal Materials, Shandong University, Jinan 250100, People's Republic of China*

Ying Da − *School of Physics, Shandong University, Jinan 250100, People's Republic of China;* orcid.org/0000-0002-8587-6874

Complete contact information is available at: https://pubs.acs.org/10.1021/acsomega.2c00048

Notes

The authors declare no competing financial interest.

■ ACKNOWLEDGMENTS

This work was financially supported by the National Natural Science Foundation of China (21972078, 21333006, and 22102087), the Natural Science Foundation of Shandong Province (ZR2019MEM004), Shandong University's multidisciplinary research and innovation team of young scholars (2020QNQT11), the Fundamental Research Funds of Shandong University (2018JC039), and the Taishan Scholar Foundation of Shandong Province.

■ REFERENCES

(1) Hakki, A.; Dillert, R.; Bahnemann, D. Photocatalytic conversion of nitroaromatic compounds in the presence of TiO_2. *Catal. Today* **2009**, *144*, 154−159.

(2) Nicolaou, K. C.; Mathison, C. J. N.; Montagnon, T. New Reactions of IBX: Oxidation of Nitrogen-and Sulfur-Containing Substrates To Afford Useful Synthetic Intermediates. *Angew. Chem., Int. Ed.* **2003**, *42*, 4077−4082.

(3) Sun, H.; Su, F.; Ni, J.; Cao, Y.; He, H.; Fan, K. Gold Supported on Hydroxyapatite as a Versatile Multifunctional Catalyst for the Direct Tandem Synthesis of Imines and Oximes. *Angew. Chem., Int. Ed.* **2009**, *48*, 4390−4393.

(4) Shiraishi, Y.; Sugano, Y.; Tanaka, S.; Hirai, T. One-Pot Synthesis of Benzimidazoles by Simultaneous Photocatalytic and Catalytic Reactions on Pt@TiO_2 Nanoparticles. *Angew. Chem., Int. Ed.* **2010**, *122*, 1700−1704.

(5) Rios-Bernÿ, O.; Flores, S. O.; Córdova, I.; Valenzuela, M. A. Synthesis of imines from nitrobenzene and TiO_2 particles suspended in alcohols via semiconductor photocatalysis type B. *Tetrahedron Lett.* **2010**, *51*, 2730−2733.

(6) Samec, J. S. M.; Éll, A. H.; Bäckvall, J. Efficient Ruthenium-Catalyzed Aerobic Oxidation of Amines by Using a Biomimetic Coupled Catalytic System. *Chem. - Eur. J.* **2005**, *11*, 2327−2334.

(7) Zavahir, S.; Zhu, H. Visible Light Induced Green Transformation of Primary Amines to Imines Using a Silicate Supported Anatase Photocatalyst. *Molecules* **2015**, *20*, 1941−1954.

(8) Dhanda, R.; Kidwai, M. Magnetically separable $CuFe_2O_4$/reduced graphene oxide nanocomposites: as a highly active catalyst for solvent free oxidative coupling of amines to imines. *RSC Adv.* **2016**, *6*, 53430−53437.

(9) Naya, S.; Kimura, K.; Tada, H. One-Step Selective Aerobic Oxidation of Amines to Imines by Gold Nanoparticle-Loaded Rutile Titanium(IV) Oxide Plasmon Photocatalyst. *ACS Catal.* **2013**, *3*, 10−13.

(10) Nicolaou, K. C.; Mathison, C. J. N.; Montagnon, T. *o*-Iodoxybenzoic Acid (IBX) as a Viable Reagent in the Manipulation of Nitrogen- and Sulfur-Containing Substrates: Scope, Generality, and Mechanism of IBX-Mediated Amine Oxidations and Dithiane Deprotections. *J. Am. Chem. Soc.* **2004**, *126*, 5192−5201.

(11) Zhu, B.; Lazar, M.; Trewyn, B. G.; Angelici, R. J. Aerobic oxidation of amines to imines catalyzed by bulk gold powder and by alumina-supported gold. *J. Catal.* **2008**, *260*, 1−6.

(12) Grirrane, A.; Corma, A.; Garcia, H. Highly active and selective gold catalysts for the aerobic oxidative condensation of benzylamines to imines and one-pot, two-step synthesis of secondary benzylamines. *J. Catal.* **2009**, *264*, 138−144.

(13) Landge, S. M.; Atanassova, V.; Thimmaiah, M.; Török, B. Microwave-assisted oxidative coupling of amines to imines on solid acid catalysts. *Tetrahedron Lett.* **2007**, *48*, 5161−5164.

(14) Mao, C.; Cheng, H.; Tian, H.; Li, H.; Xiao, W.; Xu, H.; Zhao, J.; Zhang, L. Visible light driven selective oxidation of amines to imines with BiOCl: Does oxygen vacancy concentration matter? *Appl. Catal. B: Environmental* **2018**, *228*, 87−96.

(15) Yang, J.; Mou, C. Ordered mesoporous Au/TiO_2 nanospheres for solvent-free visible-light-driven plasmonic oxidative coupling reactions of amines. *Appl. Catal. B: Environmental* **2018**, *231*, 283−291.

(16) Bai, P.; Tong, X.; Wan, J.; Gao, Y.; Xue, S. Flower-like $Bi_2O_2CO_3$-mediated selective oxidative coupling processes of amines under visible light irradiation. *J. Catal.* **2019**, *374*, 257−265.

(17) Xu, Y.; Chen, Y.; Fu, W. Visible-light driven oxidative coupling of amines to imines with high selectivity in air over core-shell structured CdS@C_3N_4. *Appl. Catal. B: Environmental* **2018**, *236*, 176−183.

(18) Huang, Y.; Chong, X.; Liu, C.; Liang, Y.; Zhang, B. Boosting Hydrogen Production by Anodic Oxidation of Primary Amines over a NiSe Nanorod Electrode. *Angew. Chem., Int. Ed.* **2018**, *57*, 13163−13166.

(19) Ding, Y.; Miao, B.; Li, S.; Jiang, Y.; Liu, Y.; Yao, H.; Chen, Y. Benzylamine oxidation boosted electrochemical water-splitting: Hydrogen and benzonitrile co-production at ultra-thin Ni_2P nanomeshes grown on nickel foam. *Appl. Catal. B: Environmental* **2020**, *268*, 118393.

(20) Kashiwagi, Y.; Kurashima, F.; Kikuchi, C.; Anzai, J.; Osa, T.; Bobbitt, J. M. Electrocatalytic Oxidation of Amines to Nitriles On a TEMPO-modified Graphite Felt Electrode (TEMPO= 2,2,6,6-tetramethylpiperidin-l -ylaxyl). *J. Chin. Chem. Soc.* **1998**, *45*, 135−138.

(21) Yu, Y.; Guo, P.; Zhong, J. S.; Yuan, Y.; Ye, K. Y. Merging photochemistry with electrochemistry in organic synthesis. *Org. Chem. Front.* **2020**, *7*, 131−135.

(22) Chiu, Y.; Lai, T.; Kuo, M.; Hsieh, P.; Hsu, Y. Photoelectrochemical cells for solar hydrogen production: Challenges and opportunities. *APL Materials* **2019**, *7*, 080901.

(23) Hardwick, T.; Qurashi, A.; Shirinfar, B.; Ahmed, N. Interfacial Photoelectrochemical Catalysis: Solar-Induced Green Synthesis of Organic Molecules. *ChemSusChem* **2020**, *13*, 1967−1973.

(24) Ru Ng, A. Y.; Boruah, B.; Chin, K. F.; Modak, J. M.; Soo, H. S. Photoelectrochemical Cells for Artificial Photosynthesis: Alternatives to Water Oxidation. *ChemNanoMat* **2020**, *6*, 185−203.

(25) Lhermitte, C. R.; Sivula, K. Alternative Oxidation Reactions for Solar-Driven Fuel Production. *ACS Catal.* **2019**, *9*, 2007−2017.

(26) Chadderdon, D. J.; Wu, L. P.; McGraw, Z. A.; Panthani, M.; Li, W. Heterostructured Bismuth Vanadate/Cobalt Phosphate Photoelectrodes Promote TEMPO-Mediated Oxidation of 5-Hydroxymethylfurfural. *ChemElectroChem.* **2019**, *6*, 3387−3392.
(27) Li, T.; Kasahara, T.; He, J.; Dettelbach, K. E.; Sammis, G. M.; Berlinguette, C. P. Photoelectrochemical oxidation of organic substrates in organic media. *Nat. Commun.* **2017**, *8*, 390.
(28) Cha, H. G.; Choi, K. Combined biomass valorization and hydrogen production in a photoelectrochemical cell. *Nat. Chem.* **2015**, *7*, 328−333.
(29) He, H.; Du, J.; Wu, B.; Duan, X.; Zhou, Y.; Ke, G.; Huo, T.; Ren, Q.; Bian, L.; Dong, F. Photoelectrochemical driving and clean synthesis of energetic salts of 5,5′-azotetrazolate at room temperature. *Green Chem.* **2018**, *20*, 3722−3726.
(30) Huang, J.; Liao, A.; Yang, D.; Wang, J.; Wu, B.; Ke, G.; Yao, W.; Zhou, Y.; He, H. Magnetic field improved photoelectrochemical synthesis of 5,5′-azotetrazolate energetic salts and hydrogen in a hematite photoanode-based cell. *Electrochim. Acta* **2020**, *330*, 135217.
(31) Liu, D.; Liu, J.; Cai, W.; Ma, J.; Yang, H. B.; Xiao, H.; Li, J.; Xiong, Y.; Huang, Y.; Liu, B. Selective photoelectrochemical oxidation of glycerol to high value-added dihydroxyacetone. *Nat. Commun.* **2019**, *10*, 1779.
(32) Vo, T.; Kao, C.; Kuo, J.; Chiu, C.; Chiang, C. Unveiling the crystallographic facet dependence of the photoelectrochemical glycerol oxidation on bismuth vanadate. *Appl. Catal. B: Environmental* **2020**, *278*, 119303.
(33) Huang, L.; Vo, T.; Chiang, C. Converting glycerol aqueous solution to hydrogen energy and dihydroxyacetone by the $BiVO_4$ photoelectrochemical cell. *Electrochim. Acta* **2019**, *322*, 134725.
(34) Abe, J. O.; Popoola, A. P. I.; Ajenifuja, E.; Popoola, O. M. Hydrogen energy, economy and storage: Review and recommendation. *Int. J. Hydrogen Energy.* **2019**, *44*, 15072−15086.
(35) Dawood, F.; Anda, M.; Shafiullah, G. M. Hydrogen production for energy: An overview. *Int. J. Hydrogen Energy* **2020**, *45*, 3847−3869.
(36) Armaroli, N.; Balzani, V. The Hydrogen Issue. *ChemSusChem* **2011**, *4*, 21−36.
(37) Sazali, N. Emerging technologies by hydrogen: A review. *Int. J. Hydrogen Energy* **2020**, *45*, 18753−18771.
(38) Zhang, H.; Li, H.; Wang, Z.; Zheng, Z.; Wang, P.; Liu, Y.; Zhang, X.; Qin, X.; Dai, Y.; Huang, B. Fabrication of $BiVO_4$ photoanode consisted of mesoporous nanoparticles with improved bulk charge separation efficiency. *Appl. Catal. B: Environmental* **2018**, *238*, 586−591.
(39) Wang, M.; Wang, Z.; Zhang, B.; Jiang, W.; Bao, X.; Cheng, H.; Zheng, Z.; Wang, P.; Liu, Y.; Whangbo, M.; et al. Enhancing the Photoelectrochemical Water Oxidation Reaction of $BiVO_4$ Photoanode by Employing Carbon Spheres as Electron Reservoirs. *ACS Catal.* **2020**, *10*, 13031−13039.
(40) Wang, S.; Chen, P.; Yun, J.; Hu, Y.; Wang, L. An Electrochemically Treated $BiVO_4$ Photoanode for Efficient Photoelectrochemical Water Splitting. *Angew. Chem., Int. Ed.* **2017**, *56*, 8500−8504.
(41) Bastin, M.; Hendrix, K.; Vankelecom, I. Solvent resistant nanofiltration for acetonitrile based feeds: A membrane screening. *J. Membr. Sci.* **2017**, *536*, 176−185.
(42) Desai, A. M.; Andreae, M.; Mullen, D. G.; Banaszak Holl, M. M.; Baker, J. R., Jr. Acetonitrile shortage: Use of isopropanol as an alternative elution system for ultra/high performance liquid chromatography. *Anal. Methods* **2011**, *3*, 56−58.
(43) McConvey, I. F.; Woods, D.; Lewis, M.; Gan, Q.; Nancarrow, P. The Importance of Acetonitrile in the Pharmaceutical Industry and Opportunities for its Recovery from Waste. *Org. Process Res. Dev.* **2012**, *16*, 612−624.
(44) Li, T.; Kasahara, T.; He, J.; Dettelbach, K. E.; Sammis, G. M.; Berlinguette, C. P. Photoelectrochemical oxidation of organic substrates in organic media. *Nat. Commun.* **2017**, *8*, 390.
(45) Tayebi, M.; Tayyebi, A.; Lee, B. K. Improved photoelectrochemical performance of molybdenum (Mo)-doped monoclinic bismuth vanadate with increasing donor concentration. *Catal. Today* **2019**, *328*, 35−42.
(46) Seabold, J. A.; Zhu, K.; Neale, N. R. Efficient solar photoelectrolysis by nanoporous Mo:$BiVO_4$ through controlled electron transport. *Phys. Chem. Chem. Phys.* **2014**, *16*, 1121−1131.
(47) Luo, W.; Li, Z.; Yu, T.; Zou, Z. Effects of Surface Electrochemical Pretreatment on the Photoelectrochemical Performance of Mo-Doped $BiVO_4$. *J. Phys. Chem. C* **2012**, *116*, 5076−5081.
(48) Tan, H.; Gu, X.; Kong, P.; Lian, Z.; Li, B.; Zheng, Z. Cyano group modified carbon nitride with enhanced photoactivity for selective oxidation of benzylamine. *Appl. Catal. B: Environmental* **2019**, *242*, 67−75.
(49) Phasayavan, W.; Japa, M.; Pornsuwan, S.; Tantraviwat, D.; Kielar, F.; Golovko, V. B.; Jungsuttiwong, S.; Inceesungvorn, B. Oxygen-deficient bismuth molybdate nanocatalysts: Synergistic effects in boosting photocatalytic oxidative coupling of benzylamine and mechanistic insight. *J. Colloid Interface Sci.* **2021**, *581*, 719−728.
(50) Zhang, Z.; Zhao, C.; Duan, Y.; Wang, C.; Zhao, Z.; Wang, H.; Gao, Y. Phosphorus-doped TiO_2 for visible light-driven oxidative coupling of benzyl amines and photodegradation of phenol. *Appl. Surf. Sci.* **2020**, *527*, 146693.
(51) Khampuanbut, A.; Santalelat, S.; Pankiew, A.; Channei, D.; Pornsuwan, S.; Faungnawakij, K.; Phanichphant, S.; Inceesungvorn, B. Visible-light-driven WO_3/BiOBr heterojunction photocatalysts for oxidative coupling of amines to imines: Energy band alignment and mechanistic insight. *J. Colloid Interface Sci.* **2020**, *560*, 213−224.
(52) Mazzaro, R.; Boscolo Bibi, S.; Natali, M.; Bergamini, G.; Morandi, V.; Ceroni, P.; Vomiero, A. Hematite nanostructures: An old material for a new story. Simultaneous photoelectrochemical oxidation of benzylamine and hydrogen production through Ti doping. *Nano Energy* **2019**, *61*, 36−46.
(53) DiMeglio, J. L.; Bartlett, B. M. Interplay of Corrosion and Photocatalysis During Nonaqueous Benzylamine Oxidation on Cadmium Sulfide. *Chem. Mater.* **2017**, *29*, 7579−7586.

https://doi.org/10.1021/acsomega.2c00048
ACS Omega 2022, 7, 12816−12824